

Article

Supercriticality, Glassy Dynamics, and the New Insight into Melting/Freezing Discontinuous Transition in Linseed Oil

Aleksandra Drozd-Rzoska , Sylwester J. Rzoska * and Joanna Łoś 

Institute of High Pressure Physics, Polish Academy of Sciences, ul. Sokółowska 29/37, 01-142 Warsaw, Poland; arzoska@unipress.waw.pl (A.D.-R.); joalos@unipress.waw.pl (J.Ł.)

* Correspondence: sylwester.rzoska@unipress.waw.pl

Abstract: The long-range supercritical changes of dielectric constant, resembling ones observed in the isotropic liquid phase of liquid crystalline compounds, are evidenced for linseed oil—although in the given case, the phenomenon is associated with the liquid–solid melting/freezing discontinuous phase transitions. This ‘supercriticality’ can be an additional factor supporting the unique pro-health properties of linseed oil. Broadband dielectric spectroscopy studies also revealed the ‘glassy’ changes of relaxation times, well portrayed by the ‘activated and critical’ equation recently introduced. In the solid phase, the premelting effect characteristic for the canonic melting/freezing discontinuous transition, i.e., without any pretransitional effect in the liquid phase, has been detected. It is interpreted within the grain model, and its parameterization is possible using the Lipovsky model and the ‘reversed’ Mossotti catastrophe concept. For the premelting effect in the solid state, the singular ‘critical’ temperature correlates with the bulk discontinuous melting and freezing temperatures. Consequently, the report shows that linseed oil, despite its ‘natural and complex’ origins, can be considered a unique model system for two fundamental problems: (i) pretransitional (supercritical) effects in the liquid state associated with a weakly discontinuous phase transition, and (ii) the premelting behavior in the solid side of the discontinuous melting/freezing discontinuous transition.

Keywords: critical phenomena; discontinuous phase transitions; premelting effect; glassy dynamics; dielectric spectroscopy; linseed oil; pro-health properties



Citation: Drozd-Rzoska, A.; Rzoska, S.J.; Łoś, J. Supercriticality, Glassy Dynamics, and the New Insight into Melting/Freezing Discontinuous Transition in Linseed Oil. *Biophysica* **2024**, *4*, 34–57. <https://doi.org/10.3390/biophysica4010003>

Academic Editor: Boris Zaslavsky

Received: 14 November 2023

Revised: 8 January 2024

Accepted: 14 January 2024

Published: 23 January 2024



Copyright: © 2024 by the authors. Licensee MDPI, Basel, Switzerland. This article is an open access article distributed under the terms and conditions of the Creative Commons Attribution (CC BY) license (<https://creativecommons.org/licenses/by/4.0/>).

1. Introduction

The extraordinary pro-health properties of flax seeds and linseed oil have been known since ancient times. Hippocrates, the ‘father’ of medicine (~400 BCE), recommended them as a significant food remedy [1]. Near 800 CE, King and Emperor Charles the Great (Charlemagne) indicated them to be essential for a healthy life in a special emperor’s mandate [2]. In modern times, Mahatma Gandhi recommended linseed oil a pro-health remedy and food addition [3]. These opinions are shared by doctors and nutritionists also nowadays [4,5]. Generally, the pro-health properties of linseed oil are explained by specific features of their components [4–23]. This report shows that yet another factor, omitted so far, can be significant: supercriticality [24–28].

It is well proven that linseed oil is an amazing pro-health food additive and a skin conditioner for natural cosmetics [11,16,21]. It can help wound healing and shows anti-inflammatory and regenerative properties [5,8,12,19,22]. It supports cardiovascular health by acting towards maintaining the required cholesterol level [7,13,17]. There are suggestions for its stimulation impact on the immune system [9,23]. The positive influence of linseed oil is broadly recognized in the fight against obesity, arthritis, and hypertension [9,13]. Focusing on cosmetics-related issues, it can strengthen skin, support redness reductions, repair skin damage (including flaky epidermis), heal skin burns and frostbite, and create smooth and soft skin [5,9,17–19,22]. Linseed is also indicated as a prophylactic anti-cancer agent for breast, colon, and prostate problems [4,17,19,23].

The bio-activity, excellent component proportions, and their synergic interactions are used to explain linseed oil's extraordinary properties [4–23]. The oil comprises polyunsaturated fatty acids (PUFA), phytoestrogenic lignans (secoisolariciresinol diglucoside, SDG), and an array of antioxidants such as phenolic acids and flavonoids. The beneficial PUFA of flax lipids are α -linolenic acid (ALA, 30–70% of the total fatty acid content), linoleic (20% of the total fatty acid content), and oleic acid (30% of the complete fatty acid content) [6,13,20].

Supercriticality means the presence of exceptional properties in the broad surrounding of the critical point, i.e., a continuous phase transition [28–31]. These properties result from the appearance and dominance of multi-molecular fluctuations associated with approaching the new phase. Their lifetime τ_{fl} and size (correlation length: ξ) show the singular, critical behavior [29]:

$$\xi(T) = \xi_0 |T - T_C|^{-\nu}, \quad (1a)$$

$$\tau_{fl}(T) = \tau_{fl}^0 |T - T_C|^{z\nu}, \quad (1b)$$

where T_C is the critical temperature, ν denotes the critical exponent for the correlation length, and z is the so-called dynamic exponent; $z = 2$ for the conserved and $z = 3$ for the non-conserved order parameter.

The 'critical quasi-phase' emerging near the critical point has led to innovative supercritical technologies, strongly developing due to their 'green' features [24–28]. They are related to the possibility of the selective extraction of components or selective chemical reactions, whose strength can be tuned by the distance from T_C . Supercriticality is indicated as a promising technology for innovative processing or microbiological preservation of food or pharmaceuticals [24,26]. Supercriticality can also promote the adhesion of some dissolved agents to the surface of solid microelements, leading to their encapsulation [24,27].

For supercritical technologies, two model relations are essential. The first one is the Kirkwood equation linking chemical reaction rate k and solubility s to the dielectric constant ε [24,28,32]:

$$k, s = p_\infty \exp \left[\frac{A\Delta_p}{RT} \left(\frac{1}{\varepsilon} - 1 \right) \right], \quad (2)$$

where Δ_p is the difference in polarity between the reactant and product, p_∞ is the prefactor related to the given property, and 'A' denotes the system-dependent constant.

The second one is the Noyes–Whitney dependence [24,28,32,33]:

$$\frac{dm}{dt} = S \frac{D}{d} C_{S-B}, \quad (3)$$

where m is the mass of the dissolved material, t is the processing time, S is the surface area of the solute particle, D is the diffusion coefficient, d is the thickness of the concentration gradient layer, and C_S and C_B are dissolving particle surface and bulk concentrations (mol/L).

In Ref. [28], the authors (SJR, ADR) converted the latter to the form containing the DC electric conductivity σ , a parameter relatively simple for experimental tests:

$$\frac{dm}{dt} = \left(\frac{k_B S}{nq^3 d} \right) T\sigma(T)(C_S - C_B) = KT\sigma(T)(C_S - C_B), \quad (4)$$

where n is the number of electric carriers/charges (q), $K = \text{const}$, k_B is the Boltzmann constant, and K is the system-dependent constant.

The above brief explanation indicates that supercriticality can be an important factor supporting, if not shaping, the unique properties of linseed oil. However, to the best of the authors' knowledge, neither communications nor suggestions regarding the appearance of the supercriticality in linseed oil or other vegetable oil have appeared.

Broadband dielectric spectroscopy (BDS) constitutes one of the basic experimental methods in studies of pretransitional properties in liquid dielectric systems [34,35]. They

are detected in the BDS spectrum via messages related to the arrangement of permanent dipole moments and the dynamics of related processes.

There are numerous reports on dielectric studies in linseed and other vegetable oils. These tests focus mainly on assessing the quality of such oils by comparing dielectric constant values or, more generally, the real part of dielectric permittivity. The results of such studies are only presented visually, with 5–10 K scanning steps, and within a limited temperature range [36–55]. The authors have not found any trial for functionally portraying dielectric constant temperature changes. Only recently dielectric constant changes have been reported in the liquid and solid phases [55]. Presented there dielectric constant changes can be related to a possible hallmark of a pretransitional effect. However, they were not discussed in such a direction [55]. Regarding dynamic dielectric properties, such as DC electric conductivity or the primary relaxation time, the Debye- or Eyring-type [33] temperature evolutions were suggested, although the mentioned limited temperature range can bias the validity of such conclusions [36,41,45,49,50,54,55].

This work presents high-resolution studies in linseed oil over a wide temperature range (~200 K). This enabled the innovative distortion-sensitive and derivative-based analysis developed by the authors [35,56–60]. The scan covered the static and dynamic domains of the complex dielectric permittivity and the hardly tested-but significant for applications—low frequency region, located below the static domain [34,60,61].

The report shows that such a ‘natural and complex’ system as linseed oil exhibits previously unknown model features regarding some fundamental and still puzzling phenomena, namely (i) in the liquid state pretransitional (supercritical) effects associated with a weakly discontinuous phase transition [29], and (ii) the premelting behavior in the solid side of the discontinuous melting/freezing transition [62].

The obtained temperature characterizations indicate a possible important role of the supercritical effect, driven by multimolecular critical fluctuations, on the unique properties of linseed oil.

2. Materials and Methods

Broadband dielectric spectroscopy (BDS) [34] measurements were performed using the Novocontrol Alpha-A impedance analyzer supplemented with a Novocontrol Quattro temperature control unit. The complex dielectric permittivity $\epsilon^* = \epsilon' - i\epsilon''$ scans were carried out in the frequency range of $1 \text{ Hz} < f < 10 \text{ MHz}$ with 5–6-digit resolution at ~230 tested temperatures, for a temperature range ca. 200 K. The real component of the dielectric permittivity was determined as $\epsilon'(f) = C(f)/C_0$, where C is the capacitance for the measurement capacitor filled with the tested sample and C_0 is for the empty capacitor. The imaginary part was calculated using the basic relation: $\epsilon''(f) = 1/2\pi f R(f) C_0$, where $R(f)$ is for the frequency-related resistivity [34]. The accuracy of the temperature stabilization was $\pm 0.1 \text{ K}$ in the basic mode, and could be improved to even $\pm 0.02 \text{ K}$. The measurement system removed all parasitic electric capacitances and was supported by the software controlling the measurement process and delivering data in the required representation, including the complex dielectric permittivity, conductivity, and modulus.

Figure A1 in Appendix A shows the obtained dielectric permittivity spectra, indicating characteristic regions manifested in frequency scans. For the static domain (in liquids, usually $1 \text{ kHz} < f < 1 \text{ MHz}$), the frequency shift does not lead to a significant change in $\epsilon'(f)$ [34]. Above the static domain, there is the relaxation domain, related to the reorientation of permanent dipole moments. Its hallmark is the primary relaxation $\epsilon''(f)$ loss curve, whose peak (maximum) estimates the primary relaxation time for basic orientational processes: $\tau = 1/2\pi f_{peak} = 1/\omega_{peak}$ [34]. It can be estimated using the derivative of experimental data via the condition $d\log_{10}\epsilon''(f = f_{max})/d\log_{10}f = 0$ [35]. It is notable that for each tested temperature even 12–15 decades in frequency could be scanned, using the impedance analyzer used in tests.

A strong rise in dielectric permittivity occurs for low frequencies, below the static domain. It can be used for determining the DC electric conductivity: $\sigma'(f) = \omega\epsilon_0\epsilon''(f) =$

$2\pi f \epsilon_0 \epsilon''(f)$ [34]. Consequently, the appearance of the horizontal, frequency-independent behavior in $\log_{10} \sigma'(f)$ vs. $\log_{10} f$ in the low-frequency (LF) domain determines and is the proof of the existence of DC electric conductivity $\sigma'(f) = \sigma$ in a given system [33]. Such behavior is presented in Figures A2 and A3 in Appendix A for the tested linseed oil. Distortions from DC electric conductivity-related behavior can be linked, for instance, to the polarization of electrodes via the Maxwell–Wagner effect [34], directly coupled to the macro-translation of ‘free’ ionic species/contaminations. The DC electric conductivity is coupled to the primary relaxation time via the Debye–Stokes–Einstein (DSE) law $\sigma(T)\tau(T) = \text{const}$. For complex systems with some ‘local structure’, the fractional (fDSE) law appears: $\sigma(T)[\tau(T)]^S = \text{const}$, where $S \neq 1$ denotes the fractional (decoupling) exponent [63].

The strong rise of the real part of the dielectric permittivity $\epsilon'(f)$ in the LF domain is often explained heuristically as the impact of non-defined residual ionic contaminations [33]. In the authors’ opinion, the phenomenon can also be explained by the translational motions of basic molecules, which supports the coupling between translational and orientational motion given in the DSE and fDSE laws [60,63]. The impedance analyzer system’s unique monitoring possibilities and the experiment’s design enabled the derivative-based and distortion-sensitive analysis of data [35,56–60].

BDS studies were carried out using a flat-parallel capacitor with gold-covered plates made from Invar (diameter $2r = 20$ mm; distance between plates $d = 0.4$ mm). The basic voltage applied in BDS measurements was $U = 1$ V. The setup (Quattro Novocontrol unit) enabled temperature control of $T = \pm 0.02$ K. Regarding the dielectric constant, values of $\epsilon'(f) = \epsilon$ for frequencies in the middle of the static domain for subsequent temperatures were taken into account, in practice shifting from ~ 10 kHz to ~ 1 kHz when cooling from 353 K to 123 K (see Appendix A). This allowed for avoidance of the biasing impacts of the low-frequency (LF) effects and high-frequency (HF) relaxation processes located below and above the static domain.

Preliminary DSC scan tests of the linseed oil between ~ 220 K and 450 K were carried out using the homemade apparatus, using $m \sim 1$ g of the sample and copper–constantan thermocouples for monitoring. The results are presented in Figure 1, overlapping those reported earlier [64–67]. This also includes DSC results at higher temperatures of $T > 450$ K, based on Ref. [65], to complete the picture. This domain is beyond the topic of the report. For the given report, the most important factor is the strong manifestation of the melting/freezing temperature.

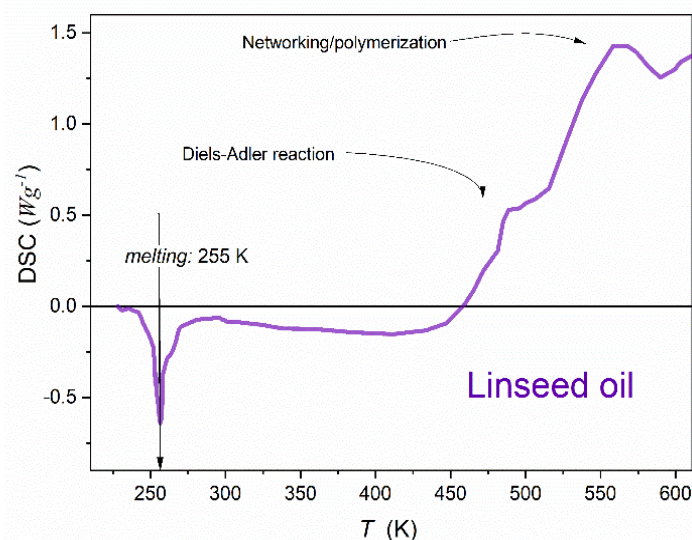


Figure 1. Differential Scanning Calorimetry (DSC) scan related to heat capacity in linseed oil (solid, purple line). Characteristic features significant for applications are indicated with arrows—the melting temperature, Diels-Adler reaction temperature and polymerization temperature.

Regarding the tested material, golden flax seeds were used from the blue-flowered flax species *Linum usitatissimum*, widely cultivated in Poland. The linseed oil was obtained via cold pressing of seeds in the laboratory. Seeds were purchased from Herbapol S.A., Lublin, Poland, the leading Polish company specializing in high-quality pro-health seeds and herb products. Triple filtering of the oils using coffee filters was carried out.

3. Comments on Critical Phenomena, Supercriticality, and Melting/Freezing Discontinuous Transition

Critical Phenomena Physics [29–31] represents one of the grand universalistic successes of 20th-century science. It explained and described common patterns appearing when approaching the critical temperature (T_C , continuous phase transition) in systems qualitatively different at the microscopic level. It covers the surroundings of the Curie temperature in magnetic or ferroelectric systems [68], liquid crystals (LCs) [29,56–60], the gas–liquid (G-L) critical point [25], mixtures of limited miscibility [30] and even relaxor ceramics [69] with ‘diffused’ paraelectric–ferroelectric transition, as shown very recently. In each case, the same general pattern for pretransitional effects of different physical magnitudes $L(T \rightarrow T_C)$ has been observed:

$$L(T) = l_0 |T - T_C|^\lambda + \dots, \quad (5)$$

where l_0 is the prefactor and λ is the critical exponent.

Critical exponents are universal, i.e., they do not depend on the microscopic properties of a given system but on such general properties as the space and order parameter dimensionalities (d, n). Moreover, only two critical exponents are independent because they are linked via a set of so-called scaling equations [29]. The mentioned universal behavior is associated with the dominance of multi-element/multi-molecular fluctuations, in which size and life grow infinitely for $T \rightarrow T_C$ (see Equations (1a) and (1b)) [29]. The name ‘supercritical’ is used for the domain above T_C , or also above the critical pressure P_C , if it is necessary for the given system [29,30]. The supercritical domain is dominated by precritical fluctuations with the symmetry of the next, more ordered phase. Pretransitional/supercritical effects are used by supercritical technologies, as discussed in the Introduction. The possibility of tuning selective solubility or chemical reaction rate by decades, simply by the distance from the critical point, is worth stressing [28,30]. So far, this technology has been explored using the supercritical domain of the gas–liquid critical point. As the ‘critical matrix’, CO_2 is most often used. It is supplemented by small amount of additional components to support reaching the desired technological target [24,26,27].

For the efficiency of supercritical technologies, the precritical anomaly of the dielectric constant and the density of the supercritical domain are important [24,26,27]. For the latter it is important that is notably larger than generally expected for the gas phase [25,28]. Consequently, one might assume that ‘using’ the supercritical region directly in a liquid phase could be optimal. However, only a single liquid–gas critical point is allowed for one-component systems, according to the Gibbs–Kohnstamm phase rule [30]. Nevertheless, in the last decades, evidence for the second liquid–liquid critical point in some liquids has appeared. Unfortunately, the related pretransitional effects are weak, and the phenomenon still constitutes a cognitive puzzle [70,71].

Notwithstanding, there is a unique case of so-called weakly discontinuous phase transitions between two fluid phases, namely isotropic liquid and nematic or smectic liquid crystalline (LC) mesophases [29,56–61]. In the given case, melting/freezing from the isotropic liquid to an LC mesophase is limited to single elements of symmetry. The characteristic feature of such systems are strong and long-range pretransitional effects, also for the temperature or pressure dependence of dielectric constant [56–61], for which the hidden in the LC mesophase extrapolated continuous phase transition T^* is the reference. Recalling Equation (5), it means the substitution of T_C with T^* , where $T^* = T_{IN} - \Delta T^*$, and T_{IN} is the isotropic–nematic ‘melting’ temperature, $\Delta T^* = 1 - 2$ K is the metric of the transition discontinuity [29,56–61]. Unfortunately, LC compounds are expensive and can

be problematic for the environmental issues. Hence, they cannot be used for supercritical technologies.

One should stress that the weakly discontinuous phase transitions constitute an exceptional case of discontinuous phase transition, with unique characterization of melting/freezing related to single elements of symmetry and long range, critical-type, pretransitional effects. They are considered within the Critical Phenomena Physics [29].

The canonic melting/freezing transition is strongly discontinuous transition, and very common in nature. Notwithstanding, it still constitutes a grand cognitive challenge despite over a century of studies [62]. In the given case, the *liquid* \leftrightarrow *crystalline solid* phase transition is not preceded by a pretransitional effect, and the basic characterization of the phenomenon is mainly the sudden jump of physical properties [62]. For some systems, weak and range-limited premelting effects in the solid state are observed upon heating from the solid phase [62,72] and refs. therein. Only recently, the authors of this report [72] noted the giant and critical-like premelting effect in solid nitrobenzene for dielectric permittivity in the static and the LF domains. The critical-like parameterization was associated with the singular ‘critical’ temperature T_m^* almost coinciding with the temperature T_m , i.e., the bulk discontinuous phase transition melting temperature. The usage of dielectric scans was essential for obtaining such evidence [72].

4. Results and Discussion

4.1. The Static Domain: Supercriticality and the Solid State Premelting and Post-Freezing Effect

There is broad evidence of dielectric studies [36–55] in edible vegetable oils, including linseed oil. They mainly focused on heuristic assessments of material quality and were carried out in limited frequency and temperature ranges. There is neither evidence nor suggestions for pretransitional or supercritical phenomena in such systems, including linseed oil. Only a hallmark can be noted in graphical presentations of results in Ref. [55].

Figure 2 presents evidence for strong and long-range supercritical changes in the dielectric constant for liquid linseed oil during cooling. Generally, the *solid* \leftarrow *liquid* phase transition reached on cooling from the liquid phase is named the freezing temperature T_f , and its value depends on the cooling rate. It links T_f to supercooling. The ‘constant’ material characterization is the melting temperature $T_m > T_f$ reached on heating from the solid phase, i.e., for *solid* \rightarrow *liquid* transition. However, for linseed oil, the same value of T_f was reached for any applied cooling rate. It facilitated reliable isothermal frequency-related BDS scans. It also indicates that for linseed oil, one can consider two material characteristics (melting temperatures) associated with *solid* \leftarrow *liquid* phase transition: $T_m^{cool} = T_f$ and $T_m^{heat} = T_m$ for *solid* \rightarrow *liquid* scans. Notably, a similar behavior was observed, for instance, in liquid crystalline isopentylcyanobiphenyl (5*CB) [73,74].

The key feature of the pretransitional/supercritical anomaly of the dielectric constant is the crossover $d\varepsilon/dT > 0 \leftarrow d\varepsilon(T_{cross})/dT = 0 \leftarrow d\varepsilon/dT < 0$ during cooling, as visible in Figures 2 and 3.

The evolution of the dielectric constant resembles the supercritical anomaly in the isotropic liquid (*I*) phase of rod-like liquid crystalline (LC) compounds on approaching LC mesophases (*M*), such as the Nematic (N), Chiral Nematic (N*), Smectic A (SmA), and Smectic E (SmE) mesophases [56–61]:

$$\varepsilon(T) = \varepsilon^* + a(T - T^*) + A(T - T^*)^\phi, \quad (6)$$

where $T > T^* = T_{I-M} - \Delta T^*$, T^* denotes the extrapolated temperature of a hypothetical continuous phase transition between the isotropic liquid (*I*) and an LC mesophase (*M*) and ΔT^* is the metric of the phase transition discontinuity, which can range from $\Delta T^* = 1 - 2$ K for the I–N transition [29,56–61] to $\Delta T^* \sim 30$ K for I–SmE transition [58]. The exponent $\phi = 1 - \alpha$, where α describes the pretransitional anomaly of the heat capacity. In the given case, $\alpha = 1/2$ and is related to the mean-field or mean-field tricritical phase transitions [29,56].

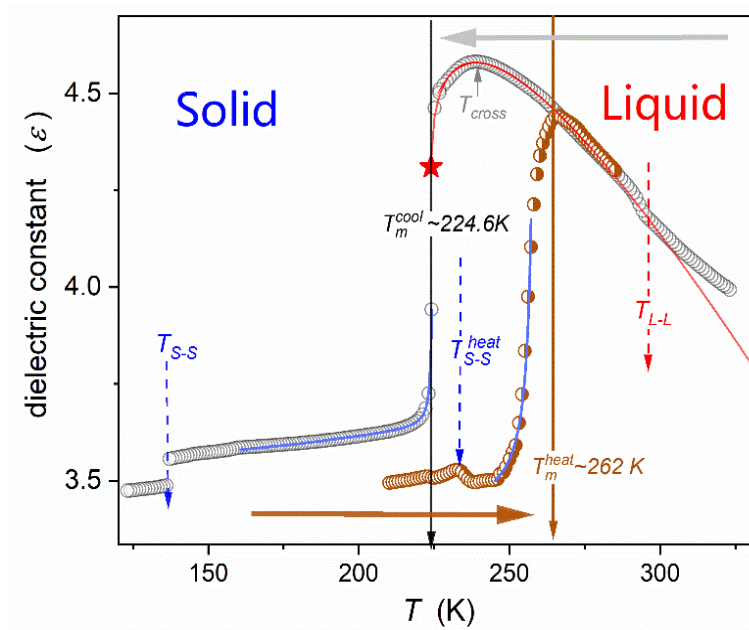


Figure 2. Temperature changes in the dielectric constant on cooling and heating in linseed oil. Note the explicit manifestations of pretransitional effects on both sides of the freezing and melting temperatures. The results are for cooling (blue, open circles) and heating (orange, semi-filled circles) cycles. The portrayal of pretransitional effects is related to Equations (6) and (9) in the liquid and solid phases, respectively. Solid vertical arrows indicate freezing and melting temperatures, respectively. The orange star indicates the extrapolated point of the continuous phase transition from the liquid to solid phase. The dashed vertical arrow indicates changes in the form of the temperature evolutions, which can eventually be associated with liquid–liquid or solid–solid transitions. The detected solid–solid (S-S) and liquid–liquid (L-L) transitions are also indicated.

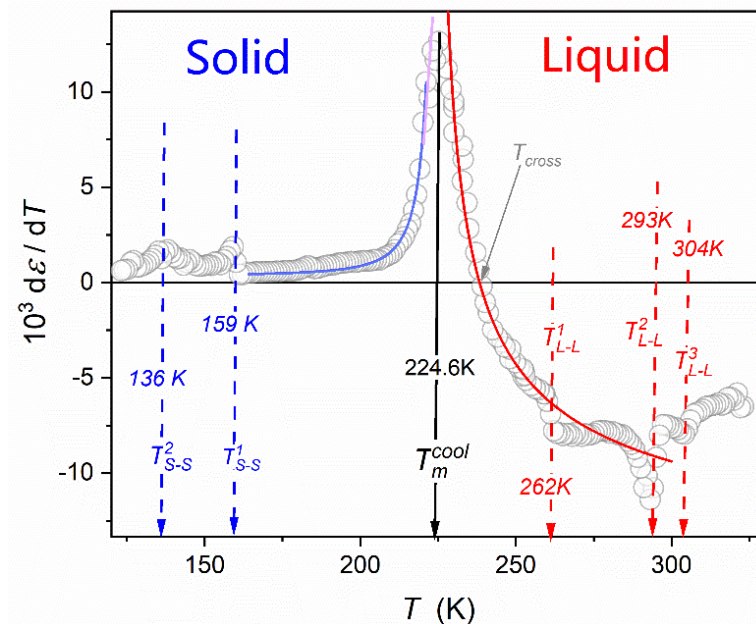


Figure 3. Temperature evolution of the derivative of the dielectric constant detected during cooling in linseed oil. Curves portraying the pretransitional behavior are related to Equation (8) (liquid phase, supercritical domain) and Equation (10) (solid phase). Values of the parameters are given in Tables 1 and 2. Note the extraordinary manifestation of the solid–solid (S-S) and liquid–liquid (L-L) transition sequences.

Table 1. Values of parameters describing pretransitional changes in the dielectric constant (Figure 2 and Equation (6)) and its derivative (Figure 3 and Equation (8)) for liquid linseed oil.

Parameter	ϵ^*	a	A	ϕ	T^*	T_m^{cool}	ΔT^*
Value	4.310	−16.4	125	0.50	224	224.6	0.6

Table 2. Values of parameters related to the post-freezing effect in the solid state, described by Equations (9) and (10), with the discontinuity metric $T^{**} = T^{**} - T_m^{cool}$.

Parameter	a (K ^{−1})	b	M (K ^{−1})	ϕ	T^{**} (K)	T_m^{cool} (K)	ΔT^{**} (K)
Value	9.3×10^{-4}	3.83	0.159	1.0	224.75	224.6	0.15

This report shows the strong pretransitional/supercritical effects in liquid linseed oil for dielectric constant and $\epsilon'(T)$ changes in the low-frequency domain. They can be well portrayed by relations used for the weakly discontinuous phase transition in LC materials [56–61]. The first ever evidence for the *liquid* → *solid* phase transition has been obtained in linseed oil and presented in Figures 1 and 2.

However, in the solid phase of linseed oil, premelting/prefreezing effects resembling ones reported for the canonic discontinuous phase transition in nitrobenzene [72] have been observed. See Figures 2–4 for the evidence of such behavior in linseed oil.

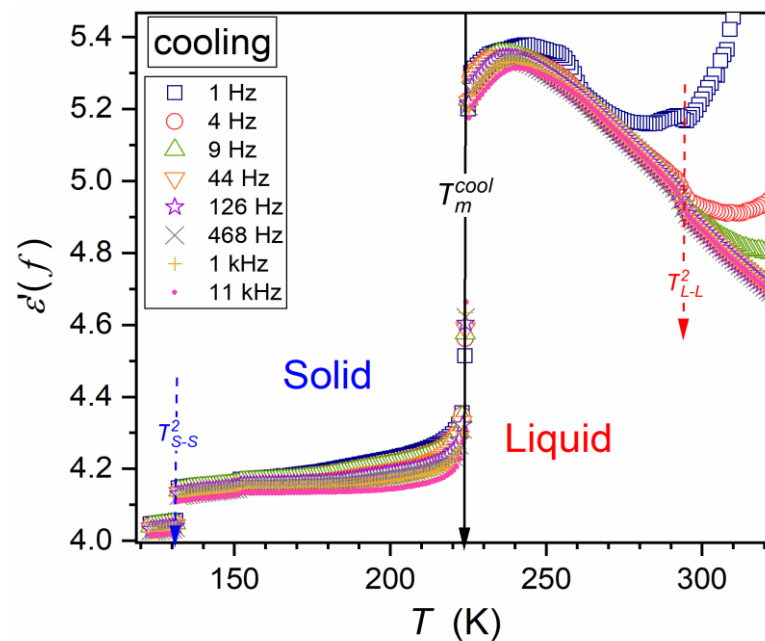


Figure 4. Temperature changes in the real part of the dielectric permittivity in linseed oil during cooling from the liquid phase for the set of frequencies from the static domain to the low-frequency (LF) domain. Arrows indicate phase transitions.

In LC materials, Equation (6) is associated with the prenematic arrangement of permanent dipole moments within pretransitional fluctuations, appearing due to the weakly discontinuous character of the phase transition. For rod-like molecules with a permanent dipole moment approximately parallel to the long molecular axis, prenematic arrangement leads to the statistical antiparallel ordering of dipole moments. Consequently, their impact on the value of the dielectric constant within fluctuations is canceled. The following relation between the dielectric constant within fluctuation and the isotropic liquid surrounding

takes place: $\varepsilon_{fluct.} \ll \varepsilon_{surrounding}$. The critical rise in the correlation length of fluctuations leads to the rise of their volume:

$$V_{fl.} \propto [\bar{\zeta}(T)]^3 \propto (T - T^*)^{-3\nu} = (T - T^*)^{-3/2}, \quad (7)$$

where $\nu = 1/2$ (mean-field value).

On approaching isotropic liquid–LC mesophase T_{I-M} discontinuous phase transition, and hence also T^* , the volume occupied by fluctuations increases, finally leading to its prevalence and the behavior described by $d\varepsilon/dT < 0$. The temperature of the isotropic liquid–LC mesophase discontinuous transition can be recognized as the symmetry-limited melting temperature, i.e., $T_{I-M} = T_m$ [56–61].

Equation (6), with the same critical exponent $\alpha = 1/2$, fairly describes the pretransitional (supercritical) behavior of the dielectric constant in linseed oil up to 80 K above the liquid–solid transition, shown in Figure 2. The weakly discontinuous phase transition can be associated with the singular temperature, linked to a hypothetical continuous phase transition: $T^* = T_m^{cool} - \Delta T^*$. It is worth stressing that a minimal value of the discontinuity metric in linseed oil: $\Delta T^* \approx 0.6$.

The portrayal of experimental data presented via Equation (6) was supported by derivative-based analysis, for which the following description of the supercritical (in the liquid phase) anomaly can be expected [57–60]:

$$\frac{d\varepsilon(T)}{dT} = a + (1 - \alpha)A(T - T^*)^{-\alpha}. \quad (8)$$

Such analysis reduces the number of fitting parameters. It is also a distortion-sensitive test, leading to a strong manifestation of pretransitional effects, as shown in Figure 3. The curves describing the supercritical effects in Figures 2 and 3 are based on simultaneous data analysis using Equations (6) and (8). The values of parameters characterizing the supercritical behavior in the liquid phase, obtained via the analysis linking Equations (6) and (8), are given in Table 1.

On heating from the solid phase a weak manifestation of $\varepsilon(T)$ premelting changes are visible in Figure 2. However for the derivative analysis presented in Figure 3, the evidence of the premelting effect is decisive, which enables a reliable parameterization. Notable in linseed oil the liquid phase is available for $T > T_m = T_m^{heat}$, located well above the crossover temperature T_{cross} . A similar behavior was obtained for dielectric constant in liquid crystalline 5*CB [73,74].

Generally, no pretransitional effects are expected in the solid phase for melting or freezing discontinuous phase transitions [62]. Notwithstanding, weak and range-limited premelting effects (i.e., during heating from the solid phase) are often observed [62,72] and refs. therein. They can be as follows [62,75–90]: (i) premelting effects are ‘weak’ and range-limited, (ii) they are detected only for some systems, (iii) they are detected for selected physical properties, (iv) there are no reports on their parameterization, except the very recent ref. [72], and (v) no solid-state pretransitional effects for freezing, i.e. on cooling from the liquid phase, are observed.

Despite the apparent limitations and problems, premelting effects are commonly considered the gateway for explaining the nature of melting/freezing discontinuous phase transitions [62,72,75–90]. This cognitive situation is qualitatively different from continuous phase transitions: understanding their origins is one of the greatest universalistic successes of 20th-century physics, as concluded in Critical Phenomena Physics [33]. Equations (1), (5) and (6) are based on this concept. Essential for success were the long-range and well-characterized pretransitional effects [29].

For melting/freezing discontinuous transitions, such pretransitional effects are (almost) absent, except for the puzzling premelting effects in the solid state [62,75–90]. In linseed oil, both premelting and post-freezing effects exist, and the latter are even stronger and longer ranged. This is evident in Figure 2 for the derivative transformation of experi-

mental data. The following relation well portrays the premelting and post-freezing effects in the solid phase of linseed oil:

$$\chi(T) = \varepsilon(T) - 1 = a + bT + \chi^0 \left| T_{m,f}^* - T \right|^{-1} \text{ for } T < T_{m,f}, \quad (9)$$

where χ denotes the dielectric susceptibility directly coupled to the electric polarization, χ^0 is the prefactor and $\chi^0 = \text{const}$, and $T_{m,f}^*$ is the ‘critical-like’ temperature almost coinciding with T_m or T_f , the background related coefficients a , $b = \text{const}$.

The derivative of Equation (9) yields:

$$\frac{d\varepsilon(T)}{dT} \approx \chi^0 \left| T_{m,f}^* - T \right|^{-2}. \quad (10)$$

The simultaneous analysis of experimental data, presented in Figures 2 and 3 led to parameters collected in Table 2 and presented graphically in the mentioned Figures.

Very recently, the behavior described by Equations (9) and (10) was also reported for the premelting effect in nitrobenzene, by the authors (ADR, SJR) [72]. The grain model, introduced for the premelting effect in the solid phase [76–81], was recalled to explain the results in ref. [72]. The model links the premelting effect to grains appearing in the solid state on heating towards T_m . Their appearance is linked to rising vibrations and defects within crystalline materials, leading to fragmentation and melting. Quasi-liquid nano-layers cover solid/crystalline grains. Lipovsky [91–93] developed the model focused on liquid nano-layers and showed their critical-like properties with the ‘critical’ temperature T_m^* almost coinciding with T_m . He derived a set of critical-like relations describing the pre-transitional evolution within liquid nano-layers. The order parameter-related susceptibility was expressed as follows [91–93]:

$$\chi_T(T) = \chi_0 (T_m^* - T)^{-\gamma'} \text{ for } T < T_m^*, \quad (11)$$

where the exponent is $\gamma' = \gamma = 1$ if the mean-field approximation obeys in the given system and T_m^* is the ‘critical’ temperature associated with the premelting effect and the quasi-liquid between crystalline grains.

Unfortunately, the liquid nano-layers occupy a ‘very tiny’ volume of the material in a premelting domain compared to dominated solid grains. This yields the essential experimental problem for the detection focused on liquid nano-layers. However, it was found in Ref. [72] that the BDS response from the liquid dielectric is qualitatively more significant than that from the solid/crystalline state. It enables the ‘extraction’ of the contribution from liquid nano-layers for a solid sample in the premelting region.

Following the reasoning presented in ref. [72], in the premelting region nano-constraints can create a quasi-negative pressure, i.e., stretching (‘rarefaction’), weakening the dipole–dipole short-range interactions for dipolar liquid. It may yield conditions appropriate for describing dielectric properties via the Clausius–Mossotti local field [94,95] conditions. Generally, this model is limited to non-dipole liquids or hypothetical dielectric systems with (almost) non-interacting permanent dipole moments [96–101]. For such a case, the so-called Mossotti Catastrophe occurs, related to the following equation [96–98]:

$$\chi(T) = \varepsilon(T) - 1 = \frac{M}{T - T_C} \text{ for } T > T_C, \quad (12)$$

where χ stands for dielectric susceptibility, directly reflecting polarization changes, T_C is the critical temperature, and M is a constant amplitude.

This paradox cannot occur in ‘normal’ liquid dielectrics [96–100]. However, conditions for its occurrence may appear in the premelting domain, as indicated above [72]. Notably, the Clausius–Mossotti local field is obeyed in ferroelectric systems, and in this case, Equation (12) is known as the Curie–Weiss equation [98,102–105]. As recently shown [69],

the validation of the Clausius–Mossotti local field is associated with the inherent uniaxiality of basic ferroelectric systems. Under such conditions, $\chi(T)$ is the susceptibility coupled to the order parameter (polarizability) [69], and Equation (12) correlates with Lipovsky's equation (Equation (11)).

For linseed oil in the solid phase, one can expect both factors, namely (i) weakening of dipole–dipole interactions due to nano-constraints and (ii) uniaxiality, which can indicate the mean-field pretransitional effect (see Equation (6)).

It is notable that in linseed oil a unique post-freezing effect exists. In the authors' opinion, it can be associated with the (very) weakly discontinuous character of the liquid–solid phase transition. For such a transition, one can expect pretransitional fluctuations on both sides of the phase transition. However, in the solid phase, they are dumped by the solidification. Notwithstanding, one can expect that on cooling below $T_f = T_m^{cool}$, the solidification/crystallization is influenced by fluctuations that have to exist due to the weakly discontinuous nature of the transition. It can support the formation of grains covered by liquid nano-layers also during cooling from the liquid phase.

4.2. The Low-Frequency Domain: Supercriticality and Premelting/Post-Freezing Effects

The value of the dielectric permittivity strongly increases when lowering frequency below the static domain. For $\varepsilon''(f, T)$, it can be discussed via the electric conductivity (see Appendix A).

The problem $\varepsilon'(f, T)$ changes in the LF domain remains puzzling, and it is most often only heuristically discussed [60] and refs. therein. Figures 4 and 5 show $\varepsilon'(f, T)$ changes in the surrounding of the liquid–solid transition down to frequencies as low as $f = 1$ Hz. In the liquid phase, evolutions of $\varepsilon(T)$ follow the pattern described by Equation (6), associated with the crossover $d\varepsilon(T)/dT > 0 \leftarrow d\varepsilon(T)/dT < 0$. The range of such behavior decreases alongside lowering of the measured frequency. This can be associated with the loss of the ability to register the presence of supercritical fluctuations, the increase in the system significant time scale described, and the rise in the observation time scale in the LF domain. The latter is proportional to the inverse of the measurement frequency.

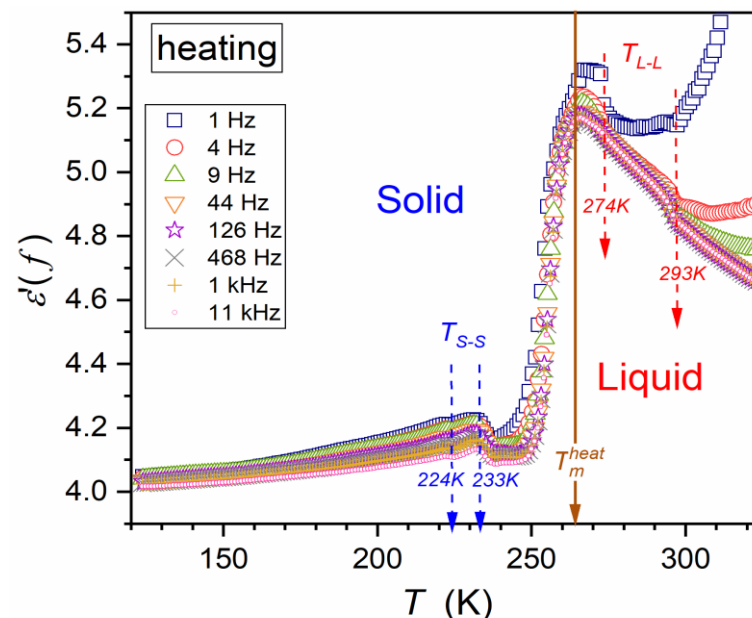


Figure 5. Temperature changes in the real part of the dielectric permittivity in linseed oil during heating from the solid phase for the set of frequencies from the static domain to the low-frequency (LF) domain. Arrows indicate directly manifesting phase transitions.

An dominated factor appearing on lowering the measurement frequency is the increase in translational processes impacts, which are negligible in the static frequency domain. This factor 'extracted' by considering the following magnitude [60,61]:

$$\Delta\epsilon'(f = \text{const}, T) = \epsilon'(f = \text{const}, T) - \epsilon'(f = 10 \text{ kHz}, T), \quad (13)$$

where $\epsilon'(f = 10 \text{ kHz}) = \epsilon$ is the reference dielectric constant with the negligible impact of translation-related contributions.

Such results for cooling and heating are presented in Figures 6 and 7, respectively.

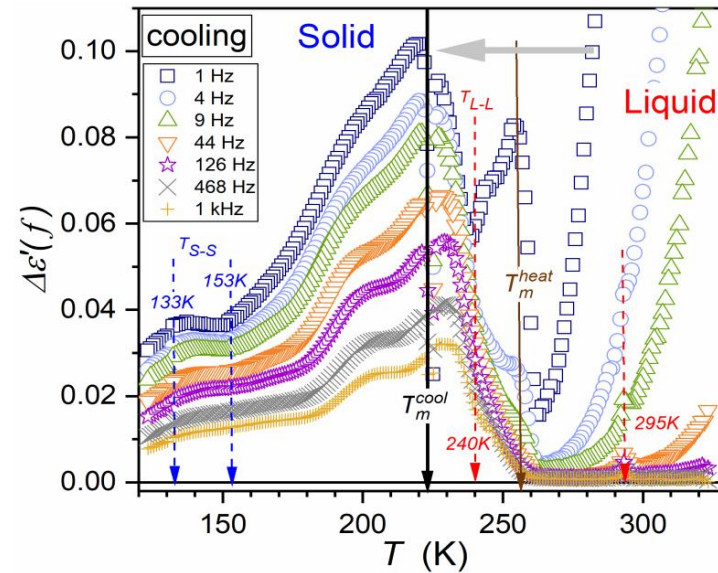


Figure 6. Linseed oil: temperature changes in the low-frequency contribution of the real part of the dielectric permittivity $\Delta\epsilon'(f) = \epsilon'(f) - \epsilon'(10 \text{ kHz})$, as obtained by subtracting the reference static value for $f = 10 \text{ kHz}$. Arrows indicate visible phase transitions.

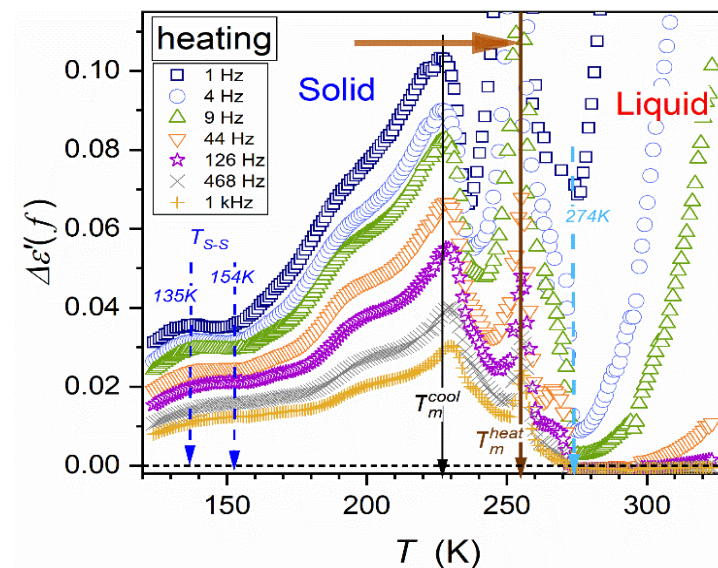


Figure 7. Linseed oil: temperature changes in the low-frequency contribution of the real part of the dielectric permittivity $\Delta\epsilon'(f) = \epsilon'(f) - \epsilon'(10 \text{ kHz})$, as obtained by subtracting the reference static value for $f = 10 \text{ kHz}$. Results for heating from the solid state are shown. Apart from the 'real' melting temperature from the solid to the liquid state (black arrow), the location of the melting (freezing) temperature obtained during cooling is indicated (light gray arrow). Arrows indicate visible phase transitions.

This contribution (Equation (13)) shows the pretransitional changes of translational processes when approaching freezing or melting temperatures. It also shows strong hallmark-changes when passing $T_m^{cool} = (T_f)$ on heating in the solid phase, despite the fact that no solid–liquid transition takes place at T_m^{cool} for such scanned path. A similar phenomenon is visible when passing T_m^{heat} for liquid-phase cooling, in the way towards T_m^{cool} .

4.3. Unique Glassy Dynamics

The real and imaginary parts of dielectric permittivity contain messages regarding the dynamics of processes. However, the analysis exploring $\epsilon''(f)$ is more convenient in practice [34] (see also Appendix A), at least in the last few decades when the modern generation of impedance analyzers have been available. The analysis of loss curves for subsequent temperatures enables the determination of primary relaxation times. For linseed oil, three relaxation processes have been detected, and these results are presented in Figure 8, using the Arrhenius scale, being the standard for showing such data [34]. Such evolutions are most often portrayed/analyzed using the Vogel–Fulcher–Tamman (VFT) super-Arrhenius equation [34,35]. However, in Ref. [35] it was shown that it is mainly an effective parameterization. It is particularly true for systems with elements of local uniaxial symmetry, and this seems to be the case of linseed oil. In fact, on the significant role of the local uniaxiality in linseed oil also indicates the pretransitional behavior of dielectric constant discussed above. In Refs. [35,106], a new route for super-Arrhenius changes of relaxation times was developed. It minimized the application of the nonlinear fitting and testing the possibility of using the selected scaling relation [35,106]. First, experimental data are transformed to the form related to the apparent activation enthalpy $H_a(T)$, or equivalently the so-called apparent fragility (steepness index) $m(T)$ [35,106]:

$$m(T) = (T_g \ln 10) H_a(T) = c H_a(T) = \frac{H}{T - T^+} \Rightarrow 1/m(T), 1/H_a(T) \propto aT - b, \quad (14)$$

where $H_a(T) = d \ln \tau(T) / d(1/T) = (d\tau(T)/\tau(T)) / d(1/T)$; originally [35] $T > T_g$ and the latter stands for the glass temperatures related to the relaxation time $\tau(T_g) = 100$ s, the amplitude $H = \text{const}$, coefficients $a, b, c = \text{const}$; the singular temperature can be determined as $1/m(T^+), 1/H_a(T^+) = 0$.

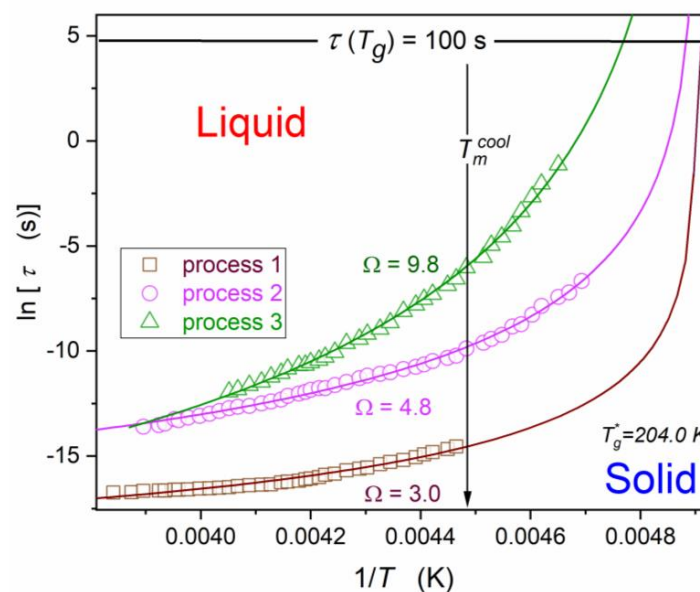


Figure 8. Temperature changes in basic relaxation processes detected for the primary loss curve for the tested linseed oil. The portrayed curves are related to ADR Equation (15) [106], with parameters given in Table 3 and supported by the derivative analysis presented in Figure 9.

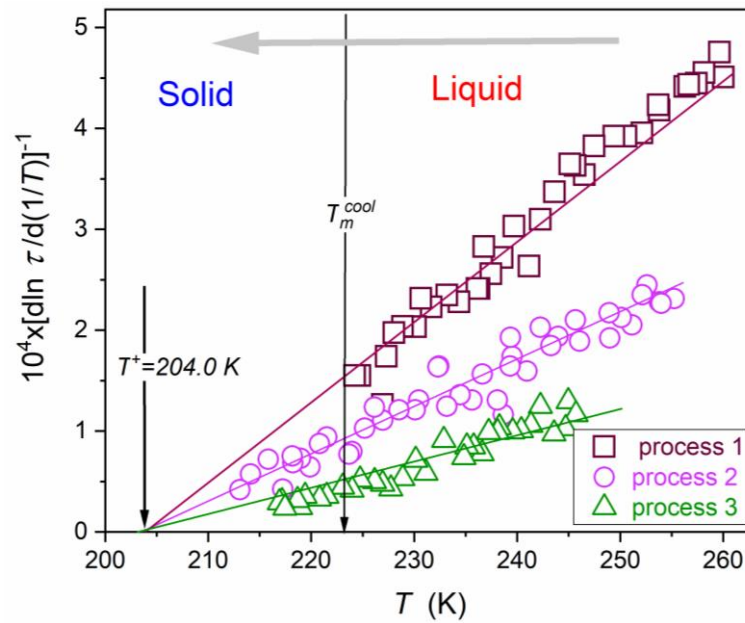


Figure 9. Temperature evolutions in the apparent activation enthalpy $H_a(T)$ reciprocals for primary relaxation processes detected in linseed oil. Solid lines are related to the universal behavior given by Equation (14). The gray arrow at the top of the figure indicates the direction of temperature change-cooling.

Table 3. Values of parameters in ADR Equation (15) describing the basic evolution of relaxation times in linseed oil, as shown graphically in Figure 8.

Parameter	$\ln C_\Omega$	Ω	T_g^* (K)	T_g (K)	ΔT_g^* (K)
Process 1	−31.1	9.85	204.0	204.5	0.5
Process 2	−22.0	4.8	204.0	206	2
Process 3	−22.2	3.0	204.0	210	6

Equation (14) was first noted for the supercooled, previtreous state of glass-forming liquids testing the evolution of the apparent fragility defined as $m(T) = d \log_{10} \tau(T) / d(T_g/T)$, where T_g is glass transition temperature defined as $\tau(T_g) = 100$ s [34,106]. The universality of Equation (14) has been proven for 18 various systems so far [35,106]. It is notable that the apparent fragility is directly proportional to the apparent enthalpy (see Equation (14)); hence, its validity can be expected for any system with the super-Arrhenius (i.e., with the temperature-dependent activation energy) system [35]. Figure 8 shows the mentioned universal behavior for three (primary) relaxation processes detected in linseed oil, with the same ‘critical’ singular temperature $T^+ \approx 204$ K. Linking the empirical finding of Equation (14) and definitions of the apparent enthalpy or the apparent fragility mentioned above, the following relation was derived by one of the authors (ADR) [106]:

$$\tau(T) = C_\Omega \left(\frac{T-T^+}{T} \right)^{-\Omega} \left[\exp \left(\frac{T-T^+}{T} \right) \right]^\Omega = C_\Omega (t^{-1} \exp(t))^\Omega \Rightarrow \ln(\tau) = \ln C_\Omega - \Omega \ln t + \Omega t, \quad (15)$$

where $t = (T - T^+)/T = 1 - T^+/T$, and T^+ stands for the ‘dynamic’ singular temperature, located below a hypothetical, hidden, glass transition.

The above relation contains only three adjustable parameters, i.e., the same ‘minimal’ number as the popular VFT equation [34]. However, the reliable value of the singular temperature T^+ can be estimated from the preliminary apparent activation enthalpy or apparent fragility analysis (see Figure 9). As shown in Ref. [106], the exponent Ω and the prefactor C_Ω also can be estimated from such a plot, reducing the final fitting of $\tau(T)$ experimental data solely to subtle adjustments. The unique form of Equation (15) is worth

indicating: it contains the critical-like and the ‘activated’ (i.e., exponential-type) terms. The solid curves in Figure 8 show the portrayal via Equation (15), with parameters collected in Table 3 and partially recalled in Figure 9. Generally, values of the exponent are located in the range $4 < \Omega < 28$, where the lower limit is typical for systems with the dominant local uniaxial symmetry [106]. The results provided in Table 3 show that for dynamic properties such as relaxation time, the behavior indicating the significant impact of the local uniaxiality exists in linseed oil.

Notably, two of three detected relaxation times can penetrate the solid phase, where they gradually diminish. A question arises if this correlates with the decay of the post-freezing effect in the solid phase, discussed above.

Figure 10 shows the temperature evolution of the DC electric conductivity, which explicitly follows the basic Arrhenius behavior, namely [36]

$$\sigma^{-1}(T) = \sigma_{\infty}^{-1} \exp\left(\frac{E_{\sigma}}{RT}\right), \quad (16)$$

with the same constant activation energy E_{σ} during cooling and heating.

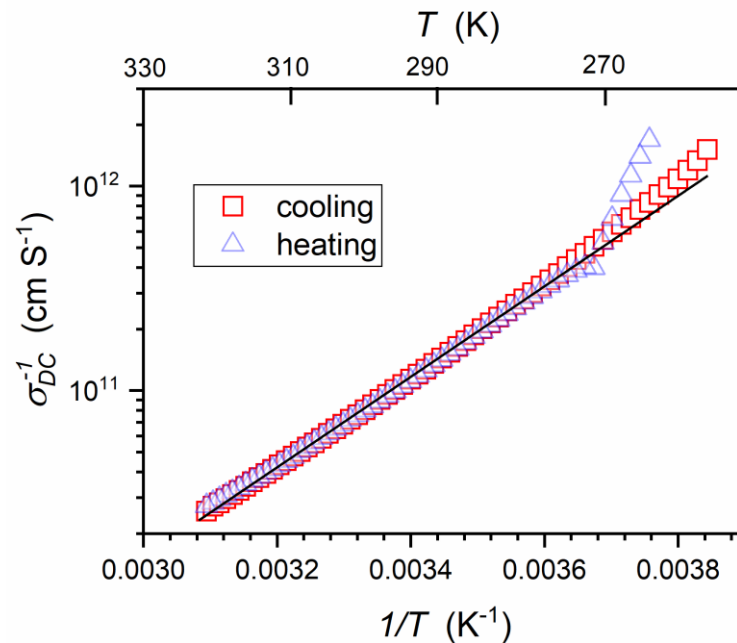


Figure 10. Temperature evolution of the reciprocal of DC electric conductivity in linseed oil during cooling (in blue) and heating (in pink). The straight line is related to the basic Arrhenius behavior. On passing $T \approx 275$ K, the crossover to the SA-type behavior appears.

The non-Arrhenius changes in relaxation time and the Arrhenius temperature changes in DC conductivity indicate the translational–orientational decoupling of these properties, as expressed via the fractional DSE law [63].

The loss factor enables insight into dynamics via the energy dissipation associated with the relaxation process, namely [97–99,107–112]

$$D = \tan\delta = \frac{i_{loss}}{i_{loss} + I} = \frac{\omega\varepsilon'' + \sigma}{\omega\varepsilon'} = \frac{1}{Q}, \quad (17)$$

where I is the total current through the sample, i_{loss} is related to its loss, and the quality factor Q is the ratio of the initial energy stored to the energy lost in one cycle for the given frequency f .

Consequently,

$$\varepsilon^* = \varepsilon' - i\varepsilon'' = \varepsilon'(1 - i \times \tan\delta). \quad (18)$$

This magnitude enables estimation of the power loss P , which can be converted to heat [97–99,107–112]:

$$P = Q \tan \delta = \omega C V^2 \tan \delta = \varepsilon_0 \varepsilon'' E^2, \quad (19)$$

where $\omega = 2\pi f$.

Results related to temperature changes in the energy loss factor for two frequencies related to the near-static and LF domains during cooling and heating are shown in Figure 11. On cooling from the liquid phase, the melting temperature is passed, since $T_f < T_m$. However, for $D = \tan \delta$, a very strong hallmark of passing T_m appears that associated with its minimum. On heating from the solid phase, one passes T_f in the solid phase on the way towards T_m and the liquid phase. In this case, a strong hallmark of passing T_f appears, which is associated with the maximum of $D = \tan \delta$. This phenomenon is frequency-dependent, as visible in Figure 11. It is notable that such a phenomenon, which has not been reported so far, is absent for the dielectric constant and primary relaxation times scans, as shown above.

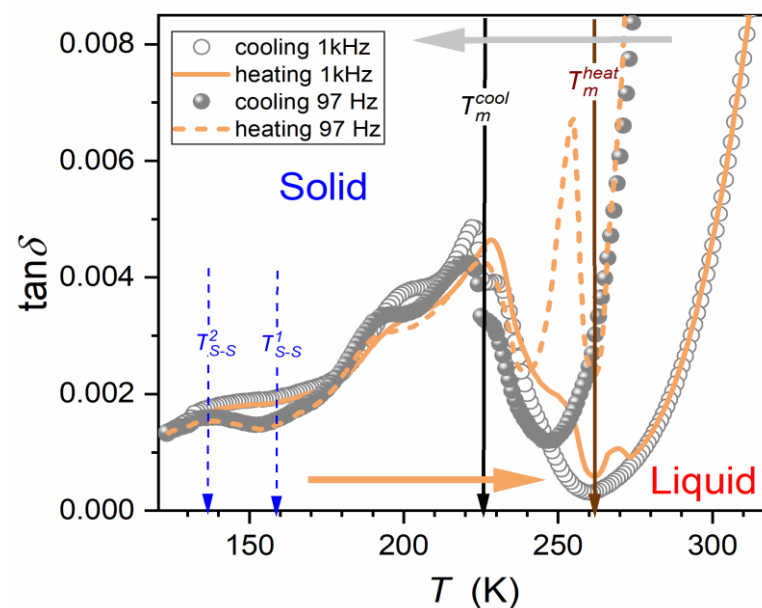


Figure 11. Temperature evolution of the loss factor $D = \tan \delta$ in linseed oil during cooling from the liquid phase and during heating from the solid phase. Note the explicit manifestations of T_m^{cool} (i.e., T_f) and T_m^{heat} (i.e., T_m), even if for the given path it is only passed without a phase transition. The gray arrow at the top of the figure and the orange one at the bottom indicate the direction of temperature change—cooling and heating respectively.

5. Conclusions

The initial motivation for carrying out the research presented in this work was to determine the precise and, so far, missing characterization of the dielectric properties of linseed oil in a broad temperature range. However, studies revealed very strong and long-range supercritical changes in the dielectric constant, resembling those observed in the isotropic liquid phase of rod-like liquid-crystalline compounds. Its influence reaches even room temperature and can be significantly greater and reach even higher temperatures thanks to admixtures that can significantly change the phase transition temperature. This is also one of the ways, apart from changing the temperature, to control the level of the discovered supercriticality in linseed oil. In current applications based on the vicinity of the liquid–gas critical point (mainly in CO_2), the area associated with this phenomenon is the basis of supercritical technologies briefly characterized in the Introduction. The unusual features related to the supercritical region and its occurrence in linseed oil raise the question of whether the unique health-promoting properties of linseed oil are related only to its components, as previously believed, and not to the influence of supercriticality.

This factor confirms the openness of innovative ‘materials engineering’ to enhance and perhaps even induce targeted effects from the health-promoting effects of linseed oil. In the case of the latter, it may be important, for example, to precisely determine the characteristics of the supercritical evolution of the dielectric constant (Equation (6)), which can be combined with the Kirkwood relation (Equation (2)). It is also possible to complete the extended Noyes–Whitney relation (Equation (4)) by determining the evolution of DC electric conductivity (Equation (16)). The possibilities mentioned here related to finding and characterizing supercritical changes in the dielectric constant in linseed oil may also have broader significance in other industrial applications of linseed oil [110–117], such as an ‘ecological’ transformer oil [110–112], for instance. They can use linseed oil as a qualitatively new and ecological supercritical carrier agent in innovative supercritical extraction or processing technologies. For these applications, it may be important that the supercritical changes in the dielectric constant in linseed oil are qualitatively more significant than in the supercritical CO₂ gas phase. Moreover, processing occurs in the liquid phase of eco-friendly natural material.

The uniqueness of the supercritical effect in linseed oil mentioned here lies in its connection with the liquid–solid discontinuous transition, which is a significant novelty. In general, melting/freezing discontinuous transition is a common and extremely important phenomenon in nature and technological applications. However, unlike continuous phase transitions, it has remained a great cognitive challenge for over 100 years. Long-range pretransitional effects and their effective parameterization became the inspiration and validation for Critical Phenomena Physics, one of the largest universal successes of 20th century physics offering the parameterization of long-range phase transition effects, being the hallmark feature of continuous/critical phase transitions. The problem with melting/freezing discontinuous transition is the practical lack of such pretransitional effects. Only weak premelting effects on heating from the solid state are detected. However, their parameterization seemed to be impossible.

Nevertheless, the premelting effect has become the main inspiration for theoretical models. A special role is played by the model of crystalline grains covered with nano-layers of a quasi-liquid, which leads to final fragmentation and melting. However, the lack of check-in relations for experimental validation has become a fundamental problem for the development of theoretical models. The exception was the Lipovsky model mentioned above. However, his predictions were for nano-layers of liquid, which were only a tiny part of melting solids, so validating the model seemed difficult, if at all possible.

This report shows that linseed oil has a premelting effect for the dielectric constant and a more significant post-freezing effect during cooling. Its parameterization is consistent with the Lipovsky model, as shown by the discussion indicating the appearance of quasi-negative pressure in nano-layers between solid grains and the Mossotti Catastrophe-type behavior. According to the authors, the unique appearance of the post-freezing effect in linseed oil may be related to the slightly discontinuous nature of the phase transition, for which ‘critical’ fluctuations should be expected to appear on both sides of the phase transition. Below T_f , it can lead to ‘granulated solidification’, with liquid nano-layers surrounding solid-state granules. Interestingly, there are hallmarks of melting on the way towards T_f for the liquid phase, as well as in the solid phase for the freezing temperature on the way towards T_m . These effects are especially visible for $D = \tan\delta$, a quantity directly related to possible energy processes in linseed oil. The results show a surprising relationship for T_f with the maximum of D and T_m with the minimum of D , with a significant frequency dependence. These changes are visible far from the mentioned characteristic temperatures. This report shows three primary relaxation processes in the liquid phase, two of them were capable of limited penetration into the solid phase. The apparent activation enthalpy associated with these relaxation times, essentially a measure of the relative changes in the relaxation time in subsequent temperature intervals, shows universal changes related to the same quasi-critical singular temperature $T_C \approx 204$ K. The facts cited in this summary indicate the importance of linseed oil as a model system of fundamental importance. It

was also important to conduct research using BDS because, with this method, the response from the liquid dielectric may be qualitatively more significant than that from the solid. For premelting and post-freezing effects in the solid state, this eliminates the problem of the tiny volume occupied by liquid nano-layers between solid-state grains.

Author Contributions: A.D.-R. proposed the concept, participated in the analysis and paper writing, and supplemented figures through data analysis; S.J.R. proposed the concept and participated in the analysis and paper writing; and J.Ł. carried out BDS studies and prepared figures. All authors have read and agreed to the published version of the manuscript.

Funding: This research was funded by the National Center for Science (NCN, Poland), grant number NCN OPUS 2022/45/B/ST5/04005, headed by S. J. Rzoska.

Data Availability Statement: All data are available directly from the authors following reasonable request. They are also deposited in the public open access database supporting data storage for research carried out at the Institute of High Pressure Physics of the Polish Academy of Sciences.

Conflicts of Interest: The authors declare no conflicts of interest.

Appendix A

Below are the results of the complex dielectric permittivity measurements during cooling in linseed oil that are presented (Figure A1) to illustrate experimental data. Basic features of the spectrum are also indicated. Figures A2 and A3 present the same data in electric conductivity presentations to show the appearance of DC electric conductivity (horizontal lines) and distortions from such behavior.

Note that the figures also indicate characteristic features of BDS spectra, both for the complex dielectric permittivity and the electric conductivity representations. For the definition of these properties and inter-relations, see the Section 2.

For presented results, features of the impedance analyzer used in the experiment and the 'design' of the experiment, described in the Section 2, are important.

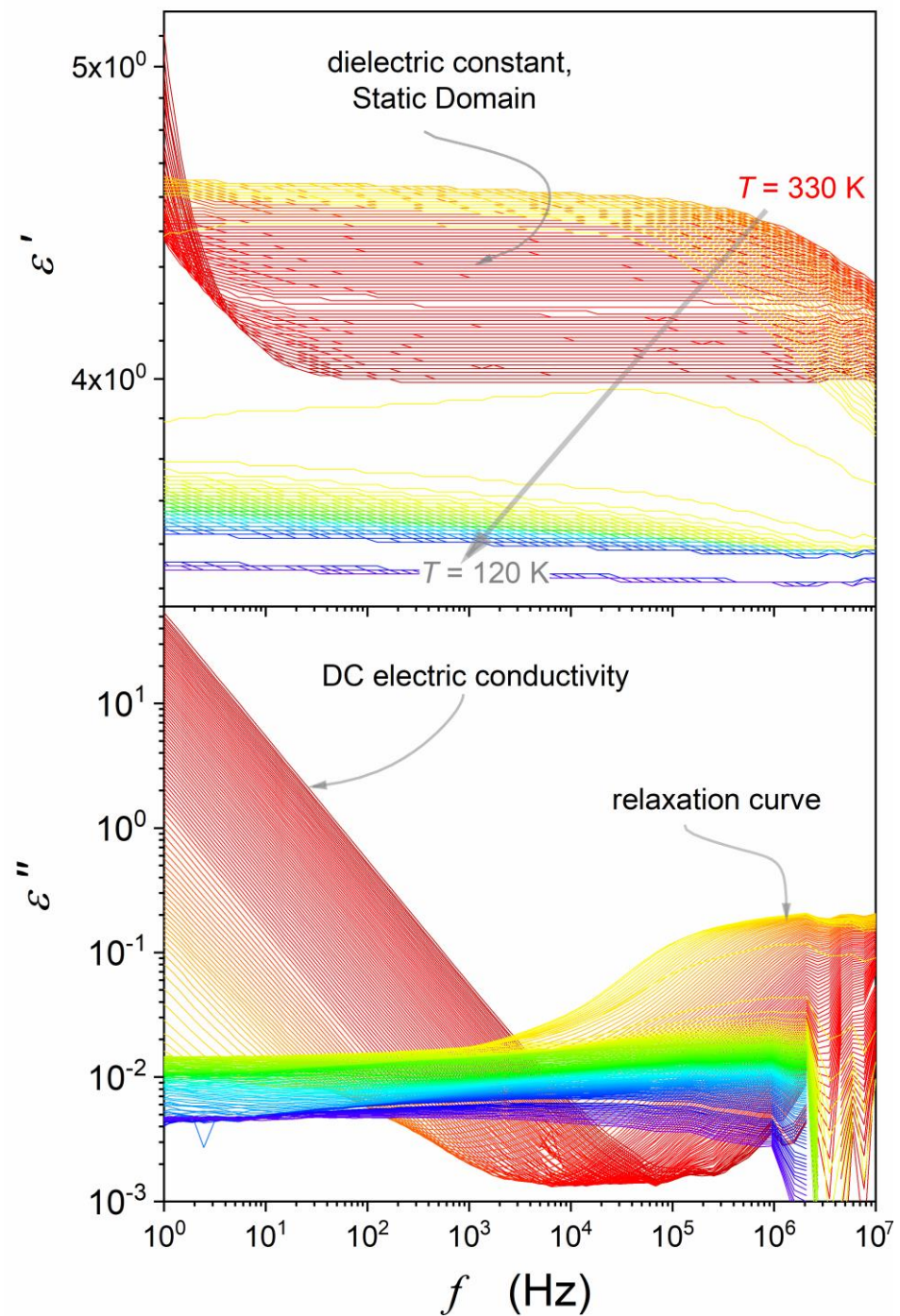


Figure A1. The real and imaginary components of the dielectric permittivity presented for the tested range of temperatures in linseed oil. The temperature shift is indicated by changing colors (from red (323 K) through yellow and green to deep blue (123 K)). Basic features of the spectrum are indicated by curved arrows. The straight arrow indicates the direction of temperature changes—cooling.

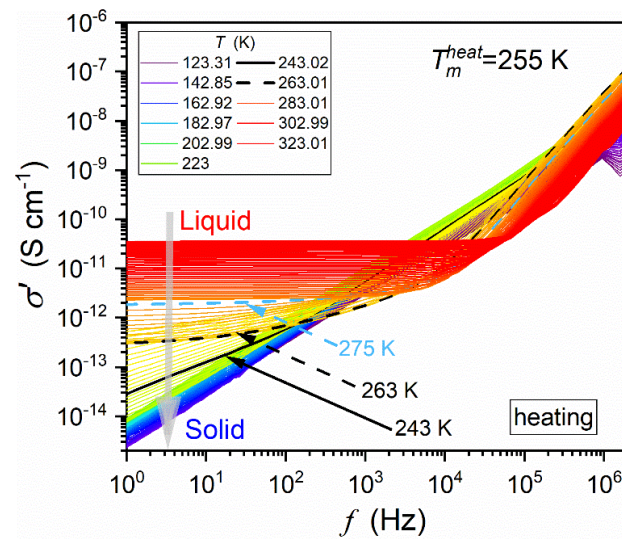


Figure A2. The real part of the complex electric conductivity obtained from $\epsilon''(f)$ experimental data collected in Figure A1. The horizontal behavior determines DC electric conductivity. The violation of such behavior is visible near melting and freezing temperatures. Results were collected during heating from the solid phase. The vertical grey arrow indicates changing temperature. The temperature shift is indicated by changing colors (from red (323 K) through yellow and green to deep blue (123 K)).

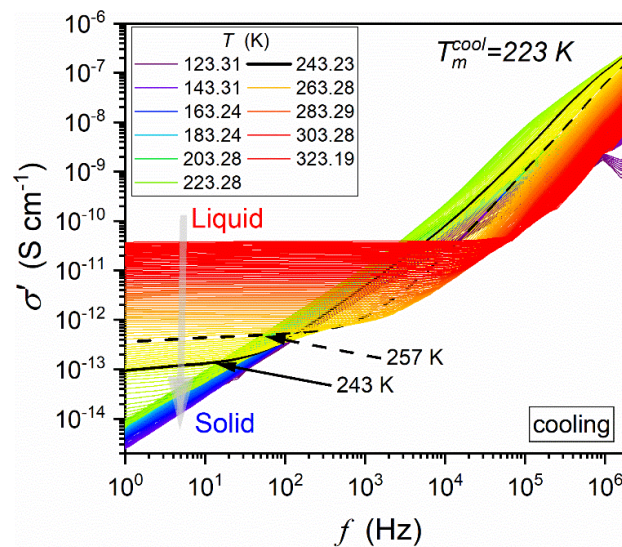


Figure A3. The real part of the complex electric conductivity obtained from $\epsilon''(f)$ experimental data collected in Figure A1 (see Section 1). The horizontal behavior determines DC electric conductivity. The violation of such behavior is visible near melting and freezing temperatures. The results were collected during cooling from the liquid phase. The straight, gray arrow indicates direction of temperature change. The temperature shift is indicated by changing colors (from red (323 K) through yellow and green to deep blue (123 K)).

References

- Flashar, H. *Meister der Heilkunst. Leben und Werk*; Beck: Berlin, Germany, 2016; ISBN 3406697461.
- Chamberlin, E.R. *The Emperor Charlemagne*; Sapere Books: Ilkley, UK, 2020; ISBN 1913518817.
- Fisher, L. *The Life of Mahatma Gandhi*; Vintage Publishing: New York, NY, USA, 2015; ISBN 1784700401.
- Johnston, I.M.; Johnston, J.R. *Flaxseed (Linseed) Oil and the Power of Omega 3*; Keats Pub. Inc.: New York, NY, USA, 1995.
- Neukam, K.; De Spirt, S.; Stahl, W.; Bejot, M.; Maurette, J.-M.; Tronnier, H.; Heinrich, U. Supplementation of flaxseed oil diminishes skin sensitivity and improves skin barrier function and condition. *Ski. Pharmacol. Physiol.* **2011**, *24*, 67–74. [[CrossRef](#)]
- Pilat, B.; Zadernowski, R. Physicochemical characteristics of linseed oil and flour. *Pol. J. Nat. Sci.* **2010**, *25*, 106–113. [[CrossRef](#)]

7. Patterson, H.B.W. *Hydrogenation of Fats and Oils*; Springer: Berlin, Germany, 2011.
8. de Souza, E.; Franco, C.M.; de Aquino, F.; Lys de Medeiros, P.; Evencio, L.B.; da Silva Goes, A.J.; de Souza Maia, M.B. Effect of a semisolid formulation of *Linum usitatissimum* L. (linseed) oil on the repair of skin wounds. *Evid.-Based Complement. Altern. Med.* **2012**, *2012*, 270752.
9. Tripathi, V.; Abidi, A.B.; Marker, S.; Bilal, S. Linseed and linseed oil: Health benefits—A review. *Int. J. Pharm. Bio. Sci.* **2013**, *3*, 434–442.
10. Bartkowski, L. Linseed—A natural source of health and beauty. *Chemik* **2013**, *67*, 186–191.
11. Goyal, A.; Sharma, V.; Upadhyay, N.; Gill, S.; Sihag, M. Flax and flaxseed oil: An ancient medicine & modern functional food. *J. Food Sci. Technol.* **2014**, *51*, 1633–1653.
12. Szymczyk, B.; Szczurek, W. Effect of dietary pomegranate seed oil and linseed oil on broiler chickens performance and meat fatty acid profile. *J. Anim. Feed Sci.* **2016**, *25*, 37–44. [[CrossRef](#)]
13. Duran, D. The pharmacological evaluation of flax seed oil. *J. Curr. Med. Res. Opin.* **2020**, *3*, 2589. [[CrossRef](#)]
14. Kiryluk, A.; Kostecka, J. Pro-environmental and health-promoting grounds for restitution of flax (*Linum usitatissimum* L.) cultivation. *J. Ecol. Eng.* **2020**, *21*, 99–107. [[CrossRef](#)] [[PubMed](#)]
15. Patel, G.; Naik, R.K.; Patel, K.K. Studies on Some Physical and Engineering Properties of Linseed. *Biol. Forum-Int. J.* **2021**, *13*, 303–308.
16. Tang, Z.-X.; Ying, R.-F.; Lv, B.-F.; Yang, L.-H.; Xu, Z.; Yan, L.-Q.; Bu, J.-Z.; Wei, Y.-S. Flaxseed oil: Extraction, health benefits and products. *Qual. Assur. Saf. Crops Foods* **2021**, *13*, 1–19. [[CrossRef](#)]
17. Li, X.; Chen, Q.; Li, Q.; Li, J.; Cui, K.; Zhang, Y.; Kong, A.; Zhang, Y.; Wan, M.; Mai, K.; et al. Effects of high levels of dietary linseed oil on the growth performance, antioxidant capacity, hepatic lipid metabolism, and expression of inflammatory genes in large yellow croaker (*Larimichthys crocea*). *Front. Physiol.* **2021**, *12*, 631850. [[CrossRef](#)]
18. Lewandowska, H.; Eljaszewicz, A.; Poplawska, I.; Tynecka, M.; Walewska, A.; Grubczak, K.; Holl, J.; Hady, H.R.; Czaban, S.L.; Reszec, J.; et al. Optimization of novel human acellular dermal dressing sterilization for routine use in clinical practice. *Int. J. Mol. Sci.* **2021**, *22*, 8467. [[CrossRef](#)] [[PubMed](#)]
19. Skórkowska-Telichowska, K.; Mierziak-Darecka, J.; Wrobel-Kwiatkowska, M.; Gebarowski, T.; Szopa, J.; Zuk, M. Wound coverage by the linen dressing accelerates ulcer healing. *Postep. Derm. Alergol* **2021**, *38*, 827–841.
20. Friend, J.N. *The Chemistry of Linseed Oil*; Legare Press: London, UK, 2022; ISBN 978-016378017.
21. Langyan, S.; Yadava, P.; Khan, F.N.; Sharma, S.; Singh, R.; Bana, R.S.; Singh, N.; Kaur, V.; Kalia, S.; Kumar, A. Trends and advances in pre- and post- harvest processing of linseed oil for quality food and health products. *Crit. Rev. Food Sci. Nutr.* **2023**, *epub ahead of print*.
22. There, U.; Gour, N.; Shrikant, S.; Choudhary, V.; Kandasamy, R. Development of skincare formulations using flaxseed oil and mucilage. *J. Pharmacogn. Phytochem.* **2023**, *12*, 33–39. [[CrossRef](#)]
23. Al-Madhagy, S.; Ashmawy, N.S.; Mamdouh, A.; Eldahshan, O.A.; Farag, M.A. A comprehensive review of the health benefits of flaxseed oil in relation to its chemical composition and comparison with other omega-3-rich oils. *Eur. J. Med. Res.* **2023**, *28*, 240. [[CrossRef](#)] [[PubMed](#)]
24. Arai, Y.; Sako, T.; Takebayashi, Y. *Supercritical Fluids: Molecular Interactions, Physical Properties and New Applications*; Springer: Berlin, Germany, 2002.
25. Drozd-Rzoska, A.; Rzoska, S.J. The super- and sub-critical effects for dielectric constant in diethyl ether. *J. Chem. Phys.* **2016**, *144*, 224506. [[CrossRef](#)] [[PubMed](#)]
26. Marszałek, K.; Doesburg, P.; Starzonek, S.; Szczepańska, J.; Woźniak, Ł.; Lorenzo, J.M.; Skąpska, S.; Rzoska, S.J.; Barba, F.J. Comparative effect of supercritical carbon dioxide and high pressure processing on structural changes and activity loss of oxidoreductive enzymes. *J. CO₂ Util.* **2019**, *29*, 46–56. [[CrossRef](#)]
27. Hong Geow, C.; Ching, M.; Tan, S.; Yeap, P.; Chin, N.L. A review on extraction techniques and its future applications in industry. *Europ. J. Lipid Sci. Technol.* **2021**, *123*, 2000302. [[CrossRef](#)]
28. Rzoska, S.J.; Drozd-Rzoska, A. Criticality-related fundamental bases for new generations of gas-liquid, liquid-liquid, and liquid (LE) extraction technologies. *Eur. Phys. J. E* **2022**, *45*, 67. [[CrossRef](#)]
29. Anisimov, M.A. *Critical Phenomena in Liquids and Liquid Crystals*; Gordon and Breach: Reading, UK, 1992.
30. Drozd-Rzoska, A.; Rzoska, S.J.; Kalabiński, J. Impact of pressure on low molecular weight near-critical mixtures of limited miscibility. *ACS Omega* **2020**, *5*, 20141–20152. [[CrossRef](#)] [[PubMed](#)]
31. Proctor, J.E. *The Liquid and Supercritical Fluid. States of Matter*; CRC Press: Boca Raton, FL, USA, 2020; ISBN 9781138589735.
32. Talevi, A.; Ruiz, M.E. Drug Dissolution: Fundamental Theoretic Models. In *The ADME Encyclopedia*; Talevi, A., Ed.; Springer: Berlin, Germany, 2022.
33. Dokoumetzidis, A.; Macheras, P. A century of dissolution research: From Noyes and Withney to the biopharmaceutics classification system. *Int. J. Pharm.* **2006**, *321*, 1–11. [[CrossRef](#)] [[PubMed](#)]
34. Kremer, F.; Schönhals, A. *Broadband Dielectric Spectroscopy*; Springer: Berlin, Germany, 2002.
35. Drozd-Rzoska, A.; Rzoska, S.J.; Starzonek, S. New scaling paradigm for dynamics in glass-forming systems. *Prog. Mater. Sci.* **2023**, *134*, 101074. [[CrossRef](#)]
36. Agrawal, S.; Bhatnagar, D. Dielectric studies of binary mixtures of edible unsaturated oils. *Indian J. Pure Appl. Phys.* **2005**, *43*, 624–629.

37. Mathew, T.; Vyas, A.D.; Tripathi, D. Dielectric properties of some edible and medicinal oils at microwave frequency. *Can. J. Pure Appl. Sci.* **2009**, *3*, 953–957.
38. Palummo, L.; Bearzotti, A. Analysis of the electrical of linseed oil films exposed humidity. *Appl. Phys. A* **2009**, *97*, 835–839. [[CrossRef](#)]
39. Shah, H.; Tahir, Q.A. Dielectric properties of vegetable oils. *J. Sci. Res.* **2011**, *3*, 48–492. [[CrossRef](#)]
40. Pecovska-Gjorgjevich, M.; Andonovski, A.; Velevska, J. Dielectric constant and induced dipole moment of edible oils subjected to conventional heating. *Maced. J. Chem. Chem. Eng.* **2012**, *31*, 285–294. [[CrossRef](#)]
41. Spohner, M.; Frk, M.; Liedermann, K. Study of electrical and rheological properties of natural and other oils. In Proceedings of the 2012 IEEE International Symposium on Electrical Insulation, San Juan, PR, USA, 10–13 June 2012; pp. 30–33.
42. Chetty, L.; Serukenya, W.I.; Ijumba, N.M. Vegetable oil based liquid nanocomposite dielectric. *S. Afr. J. Sci.* **2013**, *109*, 6. [[CrossRef](#)]
43. Khandelwal, V.; Sahoo, S.K.; Kumar, A.; Manik, G. Electrically conductive green composites based on epoxidized linseed oil and polyaniline: An insight into electrical, thermal and mechanical properties. *Compos. Part B Eng.* **2018**, *136*, 149–157. [[CrossRef](#)]
44. Xu, B.; Wei, B.; Ren, X.; Liu, Y.; Jiang, H.; Zhou, C.; Ma, H.; Chalamaiah, M.; Liang, Q.; Wang, Z. Dielectric pretreatment of rapeseed 1: Influence on the drying characteristics of the seeds and physico-chemical properties of cold-pressed oil. *Food Bioprocess Technol.* **2018**, *11*, 1236–1247. [[CrossRef](#)]
45. Kumar, A.V.P.; Goel, A.; Kumar, R.; Ojha, A.K.; John, J.K.; Joy, J. Dielectric characterization of common edible oils in the higher microwave frequencies using cavity perturbation. *J. Microw. Power Electromagn. Energy* **2019**, *53*, 48–56.
46. Woo, Y.S.; Kim, M.-J.; Lee, J.H. Prediction of oxidative stability in bulk oils using dielectric constant changes. *Food Chem.* **2019**, *279*, 216–222. [[CrossRef](#)] [[PubMed](#)]
47. Zhang, L.; Chen, J.; Jing, B.; Dong, Y.; Yu, X. New method for the discrimination of adulterated flaxseed oil using dielectric spectroscopy. *Food Anal. Methods* **2019**, *12*, 2623–2629. [[CrossRef](#)]
48. Blyagaz, A.I. Improvement of quality control methods for linseed oils. *Novye Technol. (MAJKOP)* **2019**, *1*, 11–18.
49. Teseme, W.B.; Weldelessie, H.W. Review on the study of dielectric properties of food materials. *Am. J. Eng. Technol. Manag.* **2020**, *5*, 76–83. [[CrossRef](#)]
50. Valantina, S. R Measurement of dielectric constant: A recent trend in quality analysis of vegetable oil—A review. *Trends Food Sci. Technol.* **2021**, *113*, 1–11. [[CrossRef](#)]
51. Doganer, M.; Dincer, S.; Dincer, M.S.; Duzkaya, H.; Tezcan, S.S. Statistical investigation of AC dielectric strength of flaxseed oil. In Proceedings of the 2022 IEEE 21st International Conference on Dielectric Liquids (ICDL), Sevilla, Spain, 29 May–2 June 2022; pp. 1–4.
52. Radojčić, D.; Hong, J.; Petrović, Z.S. From natural oils to epoxy resins: A new paradigm in renewable performance materials. *J. Polym. Environ.* **2022**, *30*, 765–775. [[CrossRef](#)]
53. Sudhakar, A.; Chakraborty, S.K.; Mahanti, N.K. Varghese, Advanced techniques in edible oil authentication: A systematic review and critical analysis. *Crit. Rev. Food Sci. Nutr. C* **2023**, *63*, 873–901. [[CrossRef](#)]
54. Sabnis, S.M.; Rander, D.N.; Kanse, K.S.; Joshi, Y.S.; Kumbharkhane, A.C. Spectroscopic measurement and dielectric relaxation study of vegetable oils. *Inf. Process. Agric.* **2023**, *in press*. [[CrossRef](#)]
55. Agaev, S.G.; Baida, A.A.; Georgiev, O.V.; Maiorova, O.O.; Mozyrev, A.G. Dielectric spectroscopy of vegetable oils. *Russ. J. Appl. Chem.* **2020**, *93*, 748–756. [[CrossRef](#)]
56. Drozd-Rzoska, A.; Rzoska, S.J.; Ziolo, J. Critical behaviour of dielectric permittivity in the isotropic phase of nematogens. *Phys. Rev. E* **1996**, *54*, 6452–6456. [[CrossRef](#)] [[PubMed](#)]
57. Drozd-Rzoska, A.; Rzoska, S.J.; Ziolo, J. The quasi-critical behavior of dielectric permittivity in the isotropic phase of smectogenic n-cyanobiphenyls. *Phys. Rev. E* **2000**, *61*, 5349–5354. [[CrossRef](#)] [[PubMed](#)]
58. Drozd-Rzoska, A.; Rzoska, S.J.; Czupryński, K. Phase transitions from the isotropic liquid to liquid crystalline mesophases studied by “linear” and “nonlinear” static dielectric permittivity. *Phys. Rev. E* **2000**, *61*, 5355–5360. [[CrossRef](#)] [[PubMed](#)]
59. Drozd-Rzoska, A.; Rzoska, S.J.; Pawlus, S.; Ziolo, J. Complex dynamics of supercooling n-butylcyanobiphenyl (4CB). *Phys. Rev. E* **2005**, *72*, 031501. [[CrossRef](#)] [[PubMed](#)]
60. Łoś, J.; Drozd-Rzoska, A.; Rzoska, S.J. Critical-like behavior of low-frequency dielectric properties in compressed liquid crystalline octyloxycyanobiphenyl (8OCB) and its nanocolloid with paraelectric BaTiO₃. *J. Mol. Liq.* **2023**, *377*, 121555. [[CrossRef](#)]
61. Drozd Rzoska, A.; Rzoska, S.J.; Ziolo, J.; Jadżyn, J. Quasi-critical behavior of the low-frequency dielectric permittivity in the isotropic phase of n-pentylcyanobiphenyl. *Phys. Rev. E* **2001**, *63*, 052701–052704. [[CrossRef](#)]
62. Mei, Q.S.; Lu, K. Melting and superheating of crystalline solids: From bulk to nanocrystals. *Prog. Mater. Sci.* **2007**, *52*, 1175–1262. [[CrossRef](#)]
63. Starzonek, S.; Rzoska, S.J.; Drozd-Rzoska, A.; Pawlus, S.; Biała, E.; Martinez-Garcia, J.C.; Kistersky, L. Fractional Debye-Stokes-Einstein behaviour in an ultraviscous nanocolloid glycerol and silver nanoparticles. *Soft Matter* **2011**, *11*, 5554–5562. [[CrossRef](#)]
64. Kaisersberger, E. DSC investigations of the thermal characterization of edible fats and oils. *Thermochim. Acta* **1989**, *151*, 83–90. [[CrossRef](#)]
65. Wang, C.; Erhan, S. Studies of thermal polymerization of vegetable oils with a differential scanning calorimeter. *J. Am. Oil Chem. Soc.* **1999**, *76*, 1211–1216. [[CrossRef](#)]
66. Zhang, Z.-S.; Li, D.; Zhang, L.-X.; Liu, Y.-L.; Wang, X. Heating effect on the DSC melting curve of flaxseed oil. *J. Therm. Anal. Calorim.* **2014**, *115*, 2129–2135. [[CrossRef](#)]

67. Tomaszewska-Gras, J.; Islam, M.; Grzeca, L.; Kaczmarek, A.; Fornal, E. Comprehensive thermal characteristics of different cultivars of flaxseed oil (*Linum usitatissimum* L.). *Molecules* **2021**, *26*, 1958. [[CrossRef](#)] [[PubMed](#)]
68. Murray, C. *Ferroelectric Materials: Science and Technology*; States Academic Press: Cambridge, UK, 2022; ISBN 978-1639891986.
69. Rzoska, S.J.; Drozd-Rzoska, A.; Bulejak, W.; Łoś, J.; Starzonek, S.; Szafran, M.; Gao, F. Critical insight into pretransitional behavior and dielectric tunability of relaxor ceramics. *Materials* **2023**, *16*, 7634. [[CrossRef](#)] [[PubMed](#)]
70. Mierzwa, M.; Paluch, M.; Rzoska, S.J.; Ziolo, J. The liquid-glass and liquid-liquid transitions of TPP at elevated pressure. *J. Phys. Chem. B* **2008**, *112*, 10383. [[CrossRef](#)] [[PubMed](#)]
71. Tanaka, H. Liquid-liquid transition and polyamorphism. *J. Chem. Phys.* **2020**, *153*, 130901. [[CrossRef](#)] [[PubMed](#)]
72. Kalabiński, J.; Drozd-Rzoska, A.; Rzoska, S.J. Giant premelting effects for solid-liquid discontinuous transition in nitrobenzene under compression. *Crystals* **2023**, *13*, 247. [[CrossRef](#)]
73. Rzoska, S.J.; Paluch, M.; Pawlus, S.; Drozd-Rzoska, A.; Jadzyn, J.; Czupryński, K.; Dąbrowski, R. Complex dielectric relaxation in supercooling and superpressing liquid-crystalline chiral isopentycyanobiphenyl. *Phys. Rev. E* **2003**, *68*, 031705. [[CrossRef](#)]
74. Massalska-Arodz, M.; Williams, G.I.; Smith, K.C.; Conolly, G.; Aldridge, R.A. Dabrowski. Molecular dynamics and crystallization behaviour of isopentyl cyanobiphenyl as studied by dielectric relaxation spectroscopy. *J. Chem. Soc. Faraday Trans.* **1998**, *94*, 387–394. [[CrossRef](#)]
75. Kryuchkov, N.P.; Dmitryuk, N.A.; Li, W.; Ovcharov, P.V.; Han, Y.; Sapelkin, A.V.; Yurchenko, S.O. Mean-field model of melting in superheated crystals based on a single experimentally measurable order parameter. *Sci. Rep.* **2021**, *11*, 17963. [[CrossRef](#)]
76. Riegler, H.; Köhler, R. How pre-melting on surrounding interfaces broadens solid-liquid phase transitions. *Nat. Phys.* **2007**, *3*, 890–894. [[CrossRef](#)]
77. Mishin, Y.; Boettinger, W.; Warren, J.; McFadden, G. Thermodynamics of grain boundary premelting in alloys. I. Phase-field modeling. *Acta Mater.* **2009**, *57*, 3771–3785. [[CrossRef](#)]
78. Yang, Y.; Asta, M.; Laird, B.B. Solid-liquid interfacial premelting. *Phys. Rev. Lett.* **2013**, *110*, 096102. [[CrossRef](#)] [[PubMed](#)]
79. Spatschek, R.P.; Adland, A.; Karma, A.S. Structural short-range forces between solid-melt interfaces. *Phys. Rev. B* **2013**, *87*, 024109. [[CrossRef](#)]
80. Samanta, A.; Tuckerman, M.E.; Yu, T.-Q.; Ee, W. Microscopic mechanisms of equilibrium melting of a solid. *Science* **2014**, *346*, 729–732. [[CrossRef](#)] [[PubMed](#)]
81. Rad, M.T.; Boussinot, G.; Apel, M. Dynamics of grain boundary premelting. *Sci. Rep.* **2020**, *10*, 21074.
82. Pocheć, M.; Niu, H.; Ren, L.; Bai, S.; Orzechowski, K. Premelting phenomena in n-alcohols from nonanol to dodecanol. *J. Phys. Chem. C* **2020**, *124*, 21013–21017. [[CrossRef](#)]
83. Tian, X.-L.; Zhao, Y.-H.; Peng, D.-W.; Guo, Q.-W.; Guo, Z.; Hou, H. Phase-field crystal simulation of evolution of liquid pools in grain boundary pre-melting regions. *Trans. Nonferrous Met. Soc. China* **2021**, *31*, 1175–1188. [[CrossRef](#)]
84. Azad, M.; Groulx, D.; Donaldson, A. Melting of phase change materials in horizontal annuli. *J. Energy Storage* **2021**, *42*, 103096. [[CrossRef](#)]
85. Pocheć, M.; Orzechowski, K.; Rutkowski, K. Indicators of premelting in 1-decanol and 1-nonanol studied by FTIR spectroscopy. *Surf. Interfaces* **2022**, *28*, 101676. [[CrossRef](#)]
86. Pocheć, M.; Krupka, K.M.; Panek, J.J.; Orzechowski, K.; Jezierska, A. Inside out Approach to Rotator State in Hydrogen-Bonded System-Experimental and Theoretical Cross-Examination in n-Octanol. *Int. J. Mol. Sci.* **2022**, *23*, 2138. [[CrossRef](#)]
87. Vachier, J.; Wettlaufer, J.S. Bioloocomotion and premelting in ice. *Front. Phys.* **2022**, *10*, 904836. [[CrossRef](#)]
88. Vachier, J.; Wettlaufer, J.S. Premelting controlled active matter in ice. *Phys. Rev. E* **2022**, *105*, 024601. [[CrossRef](#)] [[PubMed](#)]
89. Zhang, Q.I.; Li, W.; Qiao, K. Surface premelting and melting of colloidal glasses. *Sci. Adv.* **2023**, *9*, eadf1101. [[CrossRef](#)] [[PubMed](#)]
90. Cui, S.; Chen, H. Transition dynamics and metastable states during premelting and freezing of ice surfaces. *Phys. Rev. B* **2023**, *108*, 045413. [[CrossRef](#)]
91. Lipowsky, R. Critical surface phenomena at first-order bulk transitions. *Phys. Rev. Lett.* **1982**, *49*, 1575–1578. [[CrossRef](#)]
92. Lipowsky, R. Melting at grain boundaries and surfaces. *Phys. Rev. Lett.* **1986**, *57*, 2876. [[CrossRef](#)] [[PubMed](#)]
93. Lipovsky, T. Surface critical phenomena at first-order phase transition. *Ferroelectrics* **1987**, *73*, 69–81. [[CrossRef](#)]
94. Mossotti, O.F. Discussione analitica sull'influenza che l'azione di un mezzo dielettrico ha sulla distribuzione dell'elettricità alla superficie di più corpi elettrici disseminati. *Mem. Mat. Fis. Soc. Ital. Sci. Resid. Modena* **1850**, *24*, 49–74.
95. Clausius, R. *Die Mechanische Behandlung der Electricität*; Vieweg + Teubner Verlag: Wiesbaden, Germany, 1878.
96. Böttcher, C.J.F. *Theory of Electric Polarization*; Elsevier: Amsterdam, The Netherlands, 1973.
97. Chełkowski, A. *Dielectric Physics*; PWN-Elsevier: Warsaw, Poland, 1990.
98. von Hippel, A. *Dielectrics and Waves*; Artech House: New York, NY, USA, 1954.
99. Raju, G.G. *Dielectric in Electric Field*; CRC Press: Boca Raton, FL, USA, 2018.
100. Talebian, E.; Talebian, M. A general review on the derivation of Clausius–Mossotti relation. *Optik* **2013**, *124*, 2324–2326. [[CrossRef](#)]
101. Eremin, L.E.; Neschimenko, V.V.; Shcherbam, D.S.; Fomin, D.V. System modification of the equation Lorenz–Lorentz–Clausius Mossotti. *Optic* **2021**, *231*, 166327. [[CrossRef](#)]
102. Chen, X.; Nijhuis, C.A. The Unusual Dielectric Response of Large Area Molecular Tunnel Junctions Probed with Impedance Spectroscopy. *Adv. Electron. Mat.* **2021**, *8*, 2100495. [[CrossRef](#)]
103. Trainer, M. Ferroelectrics and the Curie–Weiss law. *Eur. J. Phys.* **2000**, *21*, 459–464. [[CrossRef](#)]
104. Hoffmann, M.; Ravindran, P.V.; Kha, A.I. Why Do Ferroelectrics exhibit negative capacitance? *Materials* **2019**, *12*, 3743. [[CrossRef](#)]

105. Mugiraneza, S.; Hallas, A.M. Tutorial: A beginner's guide to interpreting magnetic susceptibility data with the Curie-Weiss law. *Commun. Phys.* **2022**, *5*, 95. [[CrossRef](#)]
106. Drozd-Rzoska, A. Universal behavior of the apparent fragility in ultraslow glass forming systems. *Sci. Rep.* **2019**, *9*, 6816. [[CrossRef](#)] [[PubMed](#)]
107. Hill, R. Characterisation of dielectric loss in solids and liquids. *Nature* **1978**, *275*, 96–99. [[CrossRef](#)]
108. Kim, T.; Yong, H.; Kim, B.; Kim, D.; Choi, D.; Park, Y.T.; Lee, S. Energy-loss return gate via liquid dielectric polarization. *Nat. Commun.* **2018**, *9*, 1437. [[CrossRef](#)] [[PubMed](#)]
109. Morsalin, S.; Phung, T.B.; Danikas, M.; Mawad, D. Diagnostic challenges in dielectric loss assessment and interpretation: A review. *IET Sci. Meas. Technol.* **2019**, *13*, 767–782. [[CrossRef](#)]
110. Huang, Z.; Wang, F.; Wang, Q.; Yao, W.; Sun, K.; Zhang, R.; Zahao, J.; Lou, Z.; Li, J. Significantly enhanced electrical performances of eco-friendly dielectric liquids for harsh conditions with fullerene. *Nanomaterials* **2019**, *9*, 989. [[CrossRef](#)]
111. Nadolny, Z. Determination of dielectric losses in a power transformer. *Energies* **2022**, *15*, 993. [[CrossRef](#)]
112. Havran, P.; Cimbala, R.; Kurimský, J.; Dolník, B.; Kolcunová, I.; Medved, D.; Király, J.; Kohanmm, V.; Šárpataky, L. Dielectric properties of electrical insulating liquids for high voltage electric devices in a time-varying electric field. *Energies* **2022**, *15*, 391. [[CrossRef](#)]
113. Omonov, T.S.; Patel, V.R.; Curtis, J.M. Biobased thermosets from epoxidized linseed oil and its methyl esters. *ACS Appl. Polym. Mater.* **2022**, *4*, 6531–6542. [[CrossRef](#)]
114. Ruwoldt, J.; Toven, K. Alternative wood treatment with blends of linseed oil, alcohols and pyrolysis oil. *J. Bioresour. Bioprod.* **2022**, *7*, 278–287. [[CrossRef](#)]
115. Bonaduce, I.; Carlyle, L.; Colombini, M.P.; Duce, C.; Ferrari, C.; Ribechini, E.; Selleri, P.; Tiné, M.R. New insights into the ageing of linseed oil paint binder: A qualitative and quantitative analytical study. *PLoS ONE* **2012**, *7*, e49333. [[CrossRef](#)]
116. Gorée, M.; Guinée, J.B.; Huppès, G.; van Oers, L. Environmental life cycle assessment of linoleum. *Int. J. Life Cycle Assess.* **2002**, *7*, 158–166. [[CrossRef](#)]
117. Martin, D.; Saha, T.; Mcpherson, L. Condition monitoring of vegetable oil insulation in in-service power transformers: Some data spanning 10 years. *IEEE Electr. Insul. Mag.* **2017**, *33*, 44–51. [[CrossRef](#)]

Disclaimer/Publisher's Note: The statements, opinions and data contained in all publications are solely those of the individual author(s) and contributor(s) and not of MDPI and/or the editor(s). MDPI and/or the editor(s) disclaim responsibility for any injury to people or property resulting from any ideas, methods, instructions or products referred to in the content.